Statistical Inhomogeneous Broadening of Infrared and Raman Transitions in Highly Vibrationally Excited XY_6 Molecules

A. A. Makarov, I. Yu. Petrova, E. A. Ryabov, and V. S. Letokhov*

Institute of Spectroscopy, Russian Academy of Sciences, Troitsk, Moscow Region, 142092 Russia

Received: July 29, 1997; In Final Form: December 10, 1997

Simulations of the spectra of vibrational transitions in highly vibrationally excited XY_6 molecules at certain energy E_{vib} are performed. The infrared (IR) transitions in the mode ν_3 of the molecules SF_6 and WF_6 as well as the Raman ones in the mode ν_1 of SF_6 are studied. The shapes and parameters of the spectral bands, such as the integral intensity, the mean frequency, and the width, are obtained in a wide range of E_{vib}. The calculated widths prove to be much broader than the expected contributions to them because of intramolecular vibrational relaxation (IVR); this indicates the dominant role of statistical inhomogeneous broadening in the width formation for the investigated molecules.

1. Introduction

The multiple-photon (MP) excitation (E) of vibrations in and dissociation (D) of polyatomic molecules in the ground electronic state by intense IR laser pulses are at the root of a new line of inquiry in photochemistry that made its appearance thanks to the advent in the early 1970s of high-power pulsed CO_2 lasers operating in the range 9−11 μm. After the first successful experiments on the resonant action of CO_2 laser pulses upon molecular gases absorbing in the region of 10 μm,[1,2] and especially after the demonstration of the isotope-selective IR MPD of polyatomic molecules (BCl_3, SF_6),[3] there followed numerous experimental and theoretical works whose results were summarized in a series of reviews and monographs.[4−12] The interest in the IR MPE/D processes persists today because of the promise they hold for the separation of isotopes on an industrial scale in the future when reliable and economical high-power tunable pulsed IR lasers with a high repetition frequency[13] are developed.

The model of IR MPD of a polyatomic molecule is schematically illustrated in Figure 1. This qualitative model has already been discussed in the reviews and monographs cited, and here it is presented solely to make convenient the exposition of the object of the present paper. The molecule first absorbs a few IR photons in the transitions of its vibrational mode involved in the resonant interaction with the IR radiation (see the left-hand side of Figure 1). Thereafter, above some threshold energy E_{onset} (onset of vibrational chaos), there takes place the intramolecular vibrational redistribution (IVR) of the absorbed energy among the rest of the vibrational molecular modes as a result of the intermode anharmonic interaction (this is schematically shown by the broken arrows in Figure 1). This process is governed by the density of the anharmonic intermode resonances of different orders,[14−17] and it may have a multiple time scale character[18,19] at that. Finally, at the third stage, the highly excited molecule keeps absorbing the IR radiation in conditions of modification of the vibrational excitation spectrum of all the modes and the intermode anharmonicity. Qualitatively this modification boils down to the shifting of the vibrational absorption band toward the red side and its broadening as a result of the intermode anharmonicity, as illustrated schematically on the right-hand side of Figure 1. Several experimental methods aimed at studying this evolution of the vibrational absorption spectrum of polyatomic molecules are described in refs 20−23. The results of these works as well as other experimental and theoretical investigations of highly vibrationally excited molecules were summarized in ref 24 and a recent review in ref 25.

The main difficulty in comparing theory and experiment is the scarcity of data on the nature of broadening (see, for example, discussion in ref 26 related to the IR spectrum of highly vibrationally excited molecules C_2F_5I). Two effects originally contribute to the width: (1) the IVR of the energy from the vibrational mode under study (say, ν_a) which leads to the *homogeneous* broadening, and (2) the fact that molecular excitation near a certain vibrational energy E_{vib} can be represented by numerous combinations of occupation numbers of various vibrational modes which may lead to the *inhomogeneous* broadening due to different anharmonic shifts of the frequency of the mode ν_a by different combinations. The first contribution is given by the rate of IVR of the mode ν_a. In simple oscillator models, it is associated with *friction*, or *damping*, etc. For polyatomic molecules, it is calculated in the general form in refs 16 and 27. The purpose of the present work is to model theoretically only the second effect of *statistical inhomogeneous broadening* of IR and Raman transitions in polyatomic molecules. It can dominate at certain conditions, which are discussed below in section 2. It is useful to note here that, in the general stochastic theory of the line shape by Kubo,[28] such domination is referred to as the case of *slow modulation* (presuming also slow damping). On the contrary, *fast modulation* leads to the collapse of the inhomogeneous width. This collapse is analogous, in particular, to the well-known Dicke narrowing.[29] For the highly vibrationally excited molecule, the fast modulation case roughly corresponds to the fast IVR of all the modes other than ν_a (more details are in section 2), and the remaining collapsed width is associated with the rate of the *purely phase* IVR.[30,31]

We have enough indications from the experiment at present to make a statement that any of the above-mentioned effects may be mainly responsible for the broadening of spectra in

* Corresponding author. FAX: +(095)334-0886. E-mail: <letokhov@lls.isan.troitsk.ru>.

S1089-5639(97)02487-0 CCC: $15.00
Published on Web 02/10/1998

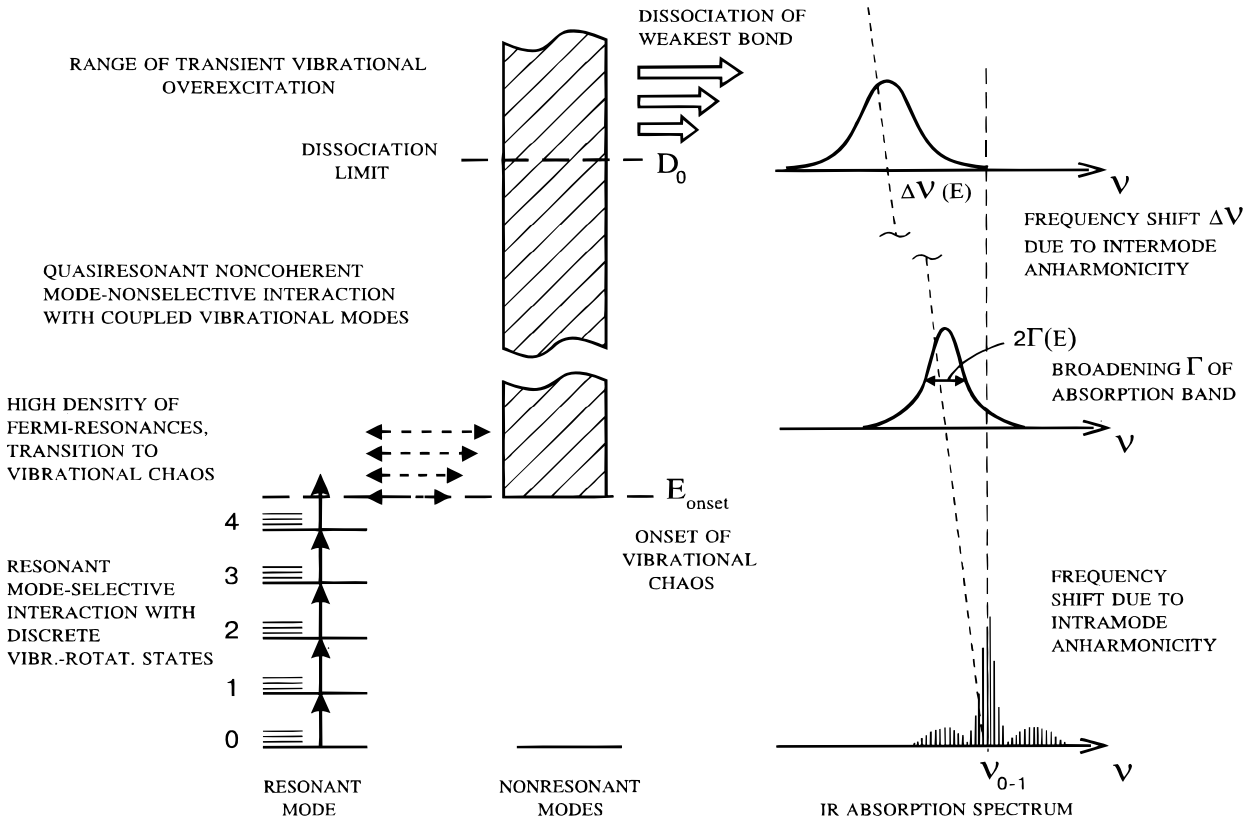

Figure 1. Main features of IR MPE/D. See the text for details.

different specific cases. Realistic arguments have been made, for example, in ref 32 in favor that the IR spectrum of mode ν_{27} in the molecule *c*-C_6F_{12} at $E_{vib} = 60\ 000\ cm^{-1}$ is broadened due to IVR of this mode. The same conclusion has been drawn in ref 21 relating to the IR spectrum of mode ν_{21} in the molecule $(CF_3)_3CI$ at $E_{vib} = 35\ 000\ cm^{-1}$. The pure dephasing width, however, gives probably the main contribution to the IR spectrum of the C−H stretching mode in the molecule $(CF_3)_3$-CH at room temperature, i.e. mean vibrational energy of about 2000 cm^{-1} (see the experimental results in ref 33 and related discussion of these results in ref 31). Eventually, inhomogeneity is considered as the principal effect in the width, at high vibrational energies, for the IR spectra of mode ν_4 of CF_3I in ref 22 and mode ν_3 of SF_6 in ref 34. We, as said above, will concentrate in this paper on the latter, just the statistical inhomogeneous broadening (in particular, for the ν_3 of SF_6).

The paper is organized as follows. Basic definitions, approximations, and equations to describe the effect of statistical inhomogeneity on spectra of vibrational transitions are given in section 2. The inhomogeneous spectral shapes can be calculated with knowledge of the fundamental frequencies ν_i of molecular vibrations and the spectroscopic anharmonicity constants x_{ij}, which are usually available from routine spectroscopy of the fundamental, combination, and overtone bands. The calculation procedure is described, in general, in section 3. Being applied to infrared transitions in the triply degenerated modes of spherical molecules like XY_6, it requires also the inclusion of anharmonic splitting. The calculation results in a wide range of vibrational energy are presented in section 4 for the molecule SF_6, and in section 5 for the molecule WF_6. The rotations are not involved up to this point. Their inclusion is made in section 6, in a simple way, after finding the nonsensitivity of previous results to the Coriolis splitting. Finally, in section 7, we discuss the reliability of calculated spectra in connection with the existing estimates on the IVR rates in SF_6.

2. Theory: Definitions and Approximations

We consider optical transitions near the frequency of one mode of a molecule (say, ν_a) which start from a vibrational state $|g_\alpha\rangle$ at some energy E_{vib}. Our assumptions and definitions are as follows.

(i) The mode ν_a is referred to as the *active mode*: it is implied that it is really active in either the infrared or the Raman spectrum, and correspondingly, the infrared or the Raman transitions are treated.

(ii) The upward transitions are considered for definiteness; this means that the absorptive infrared transitions or Stokes Raman ones are under treatment.

(iii) The other modes ν_i with $i = 1, ..., s$, where $i \neq a$, and s is the number of vibrational degrees of freedom, are referred to as the *bath modes* in accordance with the convention accepted in the literature on IVR.

(iv) The state $|g_\alpha\rangle$ is assumed to be *chaotic* (see, for example, discussion in ref 35); among other things, this means that the $|g_\alpha\rangle$ has *many* significant projections on the *regular* states $|h_\beta\rangle$, the latter being described in terms of the set of mode occupation numbers n_i with their energies $E^{(0)}_{\{n_i\}}$ near E_{vib}.

(v) Just mentioned energies of the regular states $|h_\beta\rangle \equiv |n_1, ..., n_s\rangle$ are assumed to contain the zero-order harmonic contribution and at least principal anharmonic corrections due to the spectroscopic anharmonicity constants x_{ij}, i.e.

$$E^{(0)}_\beta \equiv Ei^{(0)}_{\{n\}} \approx \sum_{i=1}^{s} n_i[\nu_i + x_{ii}(n_i - 1)] + \sum_{i=1}^{s}\sum_{j=1}^{i-1} x_{ij} n_i n_j \quad (1)$$

(vi) For illustrative purposes, we also involve some *mixing parameter* δE, a typical energy interval wherein the states $|h_\beta\rangle$ with close energies (eq 1) are strongly mixed, giving the $|g_\alpha\rangle$ as the chaotic eigenstates.

Let us consider now the upward optical transitions from the state

$$|g_\alpha\rangle = \sum_\beta c_{\beta\alpha}|h_\beta\rangle \tag{2}$$

with the energy E_α. For each basis state $|h_\beta\rangle$ entering the right side of eq 2, there is one relevant bright state $|h_\beta^{(+)}\rangle$ in the vicinity of the energy $E_{vib} + \nu_a$ which coincides with the $|h_\beta\rangle$ in all mode occupation numbers n_i except n_a, being now $n_a + 1$. Next, we include the principal anharmonic corrections to the frequency of the transition $|h_\beta\rangle \rightarrow |h_\beta^{(+)}\rangle$ according to eq 1 and use the harmonic approximation for its intensity, so the frequency is

$$\omega_\beta^{(+)} \approx \nu_a + 2x_{aa}n_a + \sum_{i\neq a} x_{ai}n_i \tag{3}$$

and intensity, in the units of the $n_a = 0 \rightarrow n_a = 1$ transition intensity, is

$$I_\beta^{(+)} \approx n_a + 1 \tag{4}$$

If the states $|h_\beta^{(+)}\rangle$ were *the eigenstates*, one would observe the spectrum of the upward transitions from the $|g_\alpha\rangle$ (see eq 2) as the lines with the frequencies $\omega_\beta^{(+)}$ (see eq 3) and the intensities $|c_{\beta\alpha}|^2 I_\beta^{(+)}$ (see eqs 2 and 4). However, they are not; the eigenstates near the energy $E_\alpha + \nu_a$ are chaotic, being some superpositions of the regular states, and transition occurs, in principle, to any upper eigenstate having a nonzero projection on any of the $|h_\beta^{(+)}\rangle$. Here we involve the mixing parameter δE and notice that, in one limited case shown in Figure 2 where spreading of the frequencies $\omega_\beta^{(+)}$ is *much wider* than the δE, the expected spectrum, in low resolution, cannot differ much from the contour of the $(\omega_\beta^{(+)}, I_\beta^{(+)})$ lines. Really, in that case of small δE, each $(\omega_\beta^{(+)}, I_\beta^{(+)})$ line may be considered as leading to some manifold of the width δE and integral intensity $I_\beta^{(+)}$, and any of such manifolds may interfere with only a small part of them. This situation may be referred to as the statistical inhomogeneity of the spectrum, since the effect results from *different* frequencies (see eq 3) of the transitions from *different* regular states giving the contributions to the initial chaotic state (eq 2). Further, being interested in the low-resolution spectrum from an ensemble of the chaotic states $|g_\alpha\rangle$ with close energies, one must do the averaging in both the α and β. As long as the equality $\sum_\alpha c_{\beta\alpha}^2 = 1$ holds true, each $\omega_\beta^{(+)}$ line is present in this spectrum as a narrow manifold of lines with its integral intensity I_β inherent in the regular state $|h_\beta\rangle$, and the searched spectrum must have the same low-resolution features as the spectrum from the ensemble of regular states near the same energy. When discussing the form of this spectrum, the term *inhomogeneous width* may be used, in particular.

We considered the case of the relatively small mixing parameter δE. The physical cause of the mixing is IVR, and roughly, the faster the IVR, the greater δE should be. Being reformulated in terms of the IVR rates γ_i, the adequate criterion (see, for example, ref 31) for the inhomogeneous broadening to dominate is a set of the inequalities

$$\gamma_i \ll \bar{n}_i\Delta_i \tag{5}$$

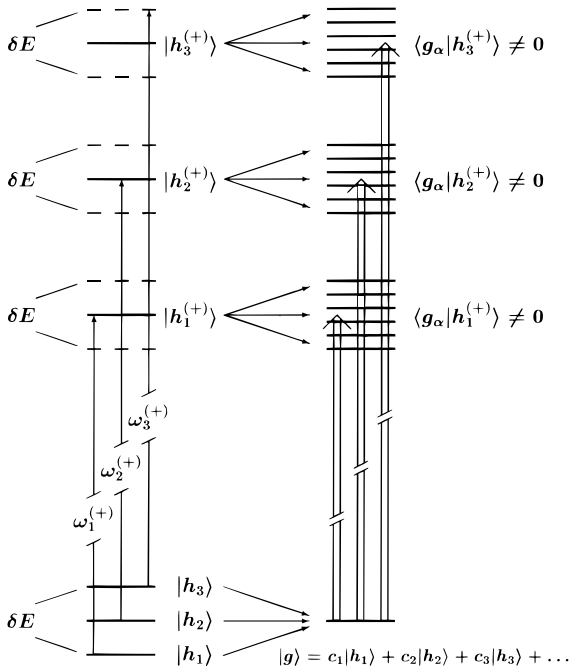

Figure 2. Illustration of the case when similarity of the spectra for the chaotic states to the inhomogeneous spectra for the ensembles of regular states may be expected. The allowed one-to-one upward transitions between the regular states $|h\rangle$ are schematically shown on the left side. The mixing of close regular states gives the chaotic states $|g\rangle$ on the right side. The optical transitions from any state $|g\rangle$ may occur to *every* chaotic state having nonzero projection onto, at least, one of the relevant $|h^{(+)}\rangle$ states.

where the following assignments are used: $\bar{n}_i$ is the mean (or equilibrium) occupation number in the ith mode at the total vibrational energy E_{vib}; γ_i describes the exponential evolution (during IVR) of the current energy in the ith mode to the equilibrium energy $\bar{n}_i\nu_i$; Δ_i is equal to the shift of the average transition frequency (eq 3) when the occupation number in the ith mode changes from n_i to $n_i + 1$ and simultaneous averaging at E_{vib} over the rest of the occupation numbers is implied. All three parameters entering the inequality eq 5 depend on E_{vib}. The $\bar{n}_i(E_{vib})$ and $\Delta_i(E_{vib})$ can be calculated numerically with knowledge of ν_i and x_{ij},[31] but evaluation of $\gamma_i(E_{vib})$ requires either the knowledge of the anharmonic coupling terms (see, for example, ref 27) and hard calculations or the experimental data and is very far from being a routine task. So, a natural way to make things clearer is to calculate the spectral shapes due to the inhomogeneous contribution; then, this should enable us to estimate how fast IVR rates cannot be ignored. Our further consideration is limited to the systems like those where the dominant role of the inhomogeneous broadening has been assumed (and probably proved) previously.[34]

3. Calculation Procedure

To simulate spectra with the dominant role of inhomogeneity, one must have tools for calculating two things as follows from the considerations of section 2. It is needed, first, to construct in explicit numerical form the representative ensemble of the regular states $|h_\beta\rangle$ lying near some energy of interest E_{vib} and, second, to get the frequencies and intensities of optical transitions from each state in the spectral region of interest. Then the resulting spectrum can be found as some average for the ensemble. Since we are interested in the spectrum also for the ensemble (now of the chaotic states also $|g_\alpha\rangle$), the averaging procedure would assume uniform contribution from all states

of the constructed ensemble and, in addition, take into account (by multiplication) their statistical weights when necessary.

Construction of the $|h_\beta\rangle$ ensemble may be *direct* or *random*. The direct procedure implies trying possible combinations of the mode occupation numbers and selecting all those states whose energy (eq 1) falls into some chosen narrow energy interval near the E_{vib}. Such procedure is computationally reasonable for small molecules, but for large molecules, it becomes expensive even with the best numerical algorithms. Of course, we tried the direct procedure for several cases of our studies below, but found that practically the same final results for the spectra could be obtained with the randomly selected ensembles which, as a rule, involved only a small part of the states near E_{vib}. We discuss, next, this random-ensemble construction and justify it in some detail.

3.1. State Ensemble Selection. The procedure starts with defining the upper and lower edges of the narrow energy interval near the current E_{vib}, usually $E_{vib} \pm \Delta E$. Then the mode occupation numbers n_i are randomly generated using some statistics, which is mathematically approved and adjusted to the E_{vib}, and each $\{n_i\}$ generation is checked to see whether the corresponding energy (eq 1) falls in the interval from $E_{vib} - \Delta E$ to $E_{vib} + \Delta E$ or not. If it does, then the generated state is included in our further calculation. The choice of the statistics must ensure the equal probabilities of generation of the nondegenerated states with equal energies. In the approximation wherein the anharmonic corrections in eq 1 are neglected, this problem can be solved using the Boltzmann statistics

$$W_i(n_i) = \left[1 - \exp\left(-\frac{\nu_i}{T}\right)\right]^{g_i} \frac{(n_i + g_i - 1)!}{n_i!(g_i - 1)!} \exp\left(-\frac{n_i\nu_i}{T}\right)$$

$$= \left[1 - \exp\left(-\frac{\nu_i}{T}\right)\right]^{g_i} G_{n_i} \exp\left(-\frac{n_i\nu_i}{T}\right) \quad (6)$$

for the independent harmonic oscillators with the frequencies ν_i and degeneracies g_i of the modes of the molecule. In fact, the probability $W(\{n_i\})$ of the $\{n_i\}$ generation divided by the corresponding state degeneracy $G(\{n_i\}) = \prod_{i=1}^{s} G_{n_i}$ depends on the sum of harmonic energies $n_i\nu_i$, only:

$$W(\{n_i\}) = \prod_{i=1}^{s} W_i(n_i) = C(T)\, G(\{n_i\}) \exp(-\sum_{i=1}^{s} n_i\nu_i) \quad (7)$$

The parameter T in eqs 6 and 7 is equivalent to the temperature and may be optimized for the rate of successful trials. The "optimum temperature" T_0 can be quite well determined by solving the equation

$$E_{vib} = \sum_{i=1}^{s} \frac{g_i\nu_i}{\exp(\nu_i/T_0) - 1} \quad (8)$$

which equalizes the current vibrational energy on the left side to the mean vibrational energy at the temperature T_0 (in the units of the Boltzmann constant) on the right side.

Choice of the window $2\Delta E$ for selection of the randomly generated states at E_{vib} is dictated by two reasons: it would be small enough for the regular dependence of the spectrum parameters on E_{vib} to be neglected inside, but would be large enough to ensure the representative statistics. The number of selected states within the $2\Delta E$ window would be also large enough to provide sufficient reproducibility of the spectrum from one computational run to another as well as quality of further smoothing procedures. These optional parameters are given below in every particular case.

In our further calculations, if there are no complete data on the anharmonicity constants (the molecule WF_6), we, selecting the generated states, limit ourselves to the harmonic approximation, for definiteness; otherwise (the molecule SF_6), we use eq 1 in full. It should be noted, however, that anharmonic corrections do not lead to any visible effects other than some evident small compression of the vibrational energy scale (see below for details).

3.2. Transition Frequencies and Intensities. Upward one-quantum vibrational transitions are under treatment in the present study, as discussed in the beginning of section 2, wherein eqs 3 and 4 are given for schematic description of the transition frequency and intensity, correspondingly. These formulas, however, are adequate just for asymmetric molecules having only nondegenarate vibrations. The XY_6 molecules being the subject of this work are spherically symmetric and belong to the point symmetry group O_h; their normal modes are usually assigned to the O_h-group irreducible representations as follows:

$$\nu_1(A_{1g}), \quad \nu_2(E_g), \quad \nu_3(F_{1u}), \quad \nu_4(F_{1u}), \quad \nu_5(F_{2g}), \quad \nu_6(F_{2u})$$

We are considering the Raman transitions in the nondegenerate mode ν_1 and infrared transitions in the 3-fold degenerate mode ν_3.

Following Hecht,[36] we write out (with minor, quite evident modifications) the diagonal second-order perturbation vibrational Hamiltonian:

$$\hat{H}_2'(\text{vib,diag}) = \sum_{i=1}^{6} X_{ii}\hat{n}_i(\hat{n}_i - 1) + \sum_{i=1}^{6}\sum_{j=1}^{i-1} X_{ij}\hat{n}_i\hat{n}_j + G_{22}\hat{m}_{2z}^{\,2} + \sum_{i=3}^{6}\sum_{j=3}^{i} G_{ij}[(\hat{\mathbf{l}}_i\cdot\mathbf{l}_j) - \hat{n}_i\delta_{ij}] + \sum_{i=2}^{6}\sum_{j=3}^{i} T_{ij}\hat{O}_{ij}(\text{tensor}) + \sum_{i=3}^{6}\sum_{j=3}^{i-1} S_{ij}\hat{O}_{ij}(\text{scalar}) \quad (9)$$

Here n_i is the ith mode occupation-number operator, $\hat{m}_{2z}$ is the operator of the vibrational angular momentum for the 2-fold degenerate mode ν_2, $\hat{\mathbf{l}}_i$ is the operator of the vibrational angular momentum for the 3-fold degenerate mode ν_i ($i = 3, \ldots, 6$), and the operators $\hat{O}_{ij}$(tensor) and O_{ij}(scalar) are some quartic combinations of the related vibrational coordinates and momenta explicitly given in ref 36. Further, in eq 9, the coefficients X_{ij}, G_{ij}, T_{ij}, and S_{ij} are, in fact, the spectroscopic anharmonicity constants: the constants X are responsible for the common shift of the manifold of states with the same set $\{n_i\}$ of vibrational quantum numbers (identically to eq (1), and the other constants are responsible for the splitting inside this manifold.

In this work, we limit ourselves to the perturbation Hamiltonian, eq 9. Transitions in the mode ν_1 are, in this approximation, described by single line of the frequency (eq 3) and intensity (eq 4) since there are no other terms than the X ones in the Hamiltonian (eq 9) coupling the mode ν_1 with the rest of the modes, so the splittings are identical in the lower and upper manifolds of the $n_1 \rightarrow n_1+1$ Raman transition. On the contrary, the infrared transition $n_3 \rightarrow n_3 + 1$ consists of some number of lines. If only the vibrational quantum number n_3 is nonzero, then the $n_3 \rightarrow n_3 + 1$ transition spectrum depends on the three constants X_{33}, G_{33}, and T_{33}. This case is studied well, and related constants can be found in literature. Knowing these constants, one can find the frequencies and intensities, which belong to any $n_3 \rightarrow n_3 + 1$ transition, in general numerically, but even

TABLE 1: $^{32}SF_6$ Spectroscopic Constants (in cm^{-1}) Used for Calculations

i	ν_i	X_{1i}	X_{2i}	X_{3i}	X_{4i}	X_{5i}	X_{6i}
1	774.5445	−0.896	−2.358	−2.902	−1.144	−1.12	−0.3625
2	643.35		−0.43	−3.603	−1.271	−0.62	−0.348
3	948.1025			−1.7468	−1.52	−1.2	−1.102
4	615.020				−0.19	+0.13	−0.1086
5	523.56					+0.85	−1.15
6	346.076						−0.8

analytically for some first n_3 values.[36] Some general features of those spectra are that the integral intensity, assuming that the split levels are populated proportionally to their degeneracies, depends on the initial n_3 as

$$I(n_3 \rightarrow n_3 + 1) = \frac{1}{3}(n_3 + 3)I(0 \rightarrow 1) \tag{10}$$

and the weight center (mean frequency) is given by

$$\bar{\nu}(n_3 \rightarrow n_3 + 1) - \nu_3 = (2X_{33} + G_{33})n_3 \tag{11}$$

That is, it is shifted from the fundamental frequency ν_3 by the value on the right side of eq 11. The effect of nonzero vibrational quantum numbers in the other modes of the molecule on the $n_3 \rightarrow n_3 + 1$ transition spectrum consists of two parts, and we encounter only one of them in this work. Namely, we assume that all the constants G_{3i}, T_{3i}, and S_{3i} ($i \neq 3$) are equal to zero. Then the spectrum in the mode ν_3 from any selected state with the set $\{n_i\}$ of the mode occupation quantum numbers takes the structure of the $n_3 \rightarrow n_3 + 1$ transition, with the current n_3 shifted additionally by

$$\Delta\nu_{\text{add}} = \sum_{i \neq 3} X_{3i} n_i \tag{12}$$

The nonzero constants G_{3i}, T_{3i}, and S_{3i} may lead to additional splittings. Our simplification is enforced to a certain extent, since these constants are far from being known in full for the molecules studied in this work. After presentation of the calculation results, we shall discuss this subject more.

4. Results for the Molecule SF_6

After some analysis of available experimental data, we have taken for calculations the values of frequencies ν_i and anharmonicity constants X_{ij} presented in Table 1. Our comments are as follows. The presented value of ν_3 is taken from ref 37; it corresponds to Hecht's definition of ν[36] and is slightly shifted from the ν_3 band origin $m(\nu_3)$ by the value $2B_0\zeta_3 \approx 0.126\ cm^{-1}$, where B_0 is the rotational constant and ζ_3 is the Coriolis constant. The other frequencies are taken from ref 38 as the band origins $m(\nu_i)$ either measured or cited therein. The intramode anharmonicity constants for the mode ν_3 are taken from ref 39, where they are obtained by the interpretation of not only the $3\nu_3$ band (as in some other works on this subject) but also the $2\nu_3 - \nu_3$ band; the constant X_{33} is given in Table 1, and two other constants are

$$G_{33} = 0.9262\ cm^{-1}, \quad T_{33} = -0.2487\ cm^{-1}$$

All other constants X_{ij} are from ref 40, where they are defined as "effective" ones and obtained from the analysis of many combination bands, but one constant X_{35} is only estimated.

Simulations of the inhomogeneous spectra in the modes ν_1 and ν_3 were performed for the energies starting from the onset of the vibrational chaos in SF_6 ($E_{\text{onset}} \simeq 5000\ cm^{-1}$ [41]) up to the dissociation limit, which is about 32 000 cm^{-1} [42].

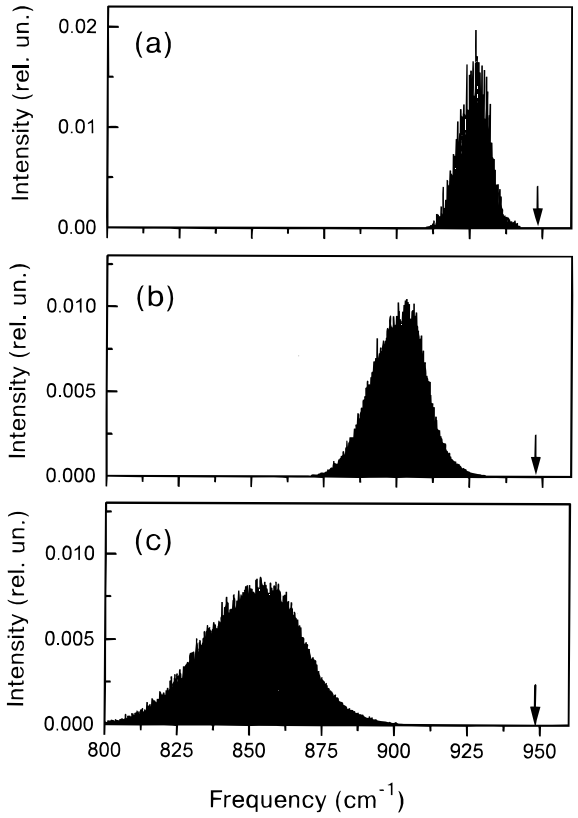

Figure 3. Histograms of the intensity distribution of the upward transitions in the ν_3 mode of SF_6 for different vibrational energies: (a) 7000 cm^{-1}; (b) 15000 cm^{-1}; (c) 30000 cm^{-1}. The fundamental frequency is indicated by the arrow.

4.1. Mode ν_3. As said above in section 3, our calculation of the spectrum starts from the selection of a certain number of vibrational states within the $2\Delta E$ interval near the energy E_{vib}. The value $\Delta E = 50\ cm^{-1}$ was used in all our computations. The reason for this choice was that the narrower ΔE (even down to 1 cm^{-1}) did not show any significant difference in the resulting spectral contour parameters for any energy E_{vib}. In addition, the procedure of selection of the states, falling into this energy interval ΔE, from the randomly generated ones turned out to be fast enough to deal with the large ensembles, usually about 10^4 states.

The spectral distribution (histogram) of transition intensities is shown in Figure 3 for three energies $E_{\text{vib}} = 7000\ cm^{-1}$ (a), $E_{\text{vib}} = 15\,000\ cm^{-1}$ (b), and $E_{\text{vib}} = 30\,000\ cm^{-1}$ (c). Each of these histograms presents intensities of all allowed transitions from the states selected in one computational run divided by the number of these states (10 000 for Figure 3a, 10 000 for Figure 3b, and 5000 for Figure 3c). Therefore, the aggregate intensity of the histogram is equal to $(\bar{n}_3 + 3)/3$ in the units of the $0 \rightarrow 1$ transition intensity (see eq 10) with the mode ν_3 mean occupation number $\bar{n}_3$ just for that run. One can see from the presented histograms the evolution of the transition spectrum: the higher the energy E_{vib}, the more intense, broadened, and red-shifted this spectrum is. Of course, the histogram characteristics at some energy E_{vib} fluctuate from run to run, but these fluctuations naturally drop ($\propto N_{\text{run}}^{-1/2}$) as the number N_{run} of selected states is increased. Such parameters of the spectrum as its integral intensity, mean frequency, and typical width converge to some well-defined values which, in addition, do not depend on ΔE.

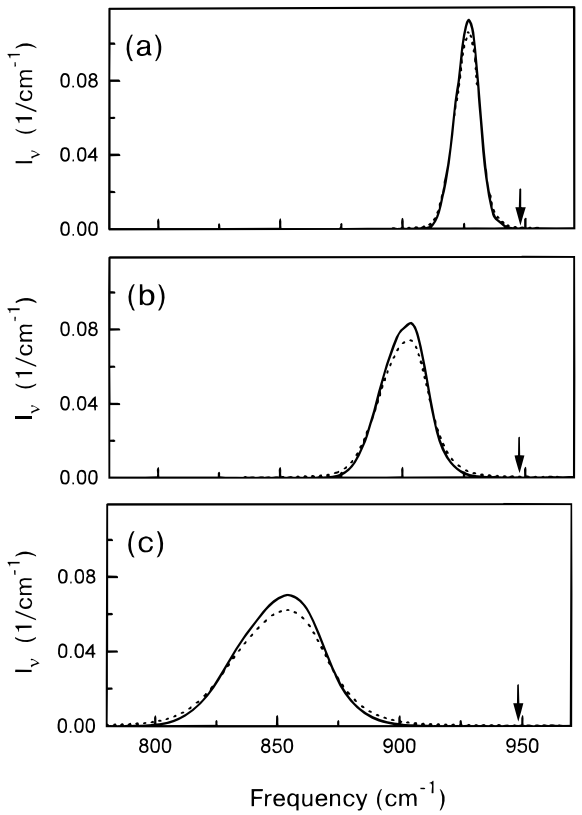

Figure 4. Upward transition spectra in the ν_3 mode of SF_6 for different vibrational energies: (a) 7000 cm^{-1}; (b) 15000 cm^{-1}; (c) 30000 cm^{-1}. The solid lines present the results of convolution of the histograms in Figure 3 with the Gaussian windows of the width $2\sigma_{Gw}$ equal to 1.5 cm^{-1} (a), 2.7 cm^{-1} (b), and 5.4 cm^{-1} (c). The dashed lines present the results of convolution of the same histograms with the Lorentzians of the widths $2\gamma_L$ equal to 1 cm^{-1} (a), 3 cm^{-1} (b), and 6 cm^{-1} (c).

Now, we discuss how the histograms, as shown in Figure 3, are further processed for determination of the spectral contour parameters. Here it should be noted that we are treating spectra with the dominant role of inhomogeneity, but the *chaotic spectra*, nevertheless. The latter means that each transition in the histogram represents, in fact, some relatively narrow substructure due to the mixing of the regular states (see the discussion in section 2 illustrated schematically by Figure 2). From the very general considerations outlined also in section 2, the mentioned substructure is expected to be of Lorentzian-contour type. So, the natural procedure of smoothing histograms is their convolution with the Lorentzian. It is preferable to use some realistic Lorentzian halfwidth, γ_L, and the halfwidths estimated by Angelié[34] for the case under consideration from his own experimental results[43] have been used. In addition, to extract the net result of the statistical inhomogeneity, the convolution with the narrow Gaussian window has been done. Its width $2\sigma_{Gw}$ was taken to ensure histogram smoothing as well as to add to the histogram width not more than several percent. Particular values of $2\sigma_{Gw}$ are given in the captions for the relevant figures.

The results of these convolutions are shown in Figure 4. This figure presents the transition spectra [the spectral density $I_\nu(\nu)$ of the transition intensity] for the same energies as in Figure 3. As mentioned earlier for the histograms, the transition spectrum becomes broader and shifts to the red side when the energy of the molecule E_{vib} goes up. The resulting spectral shape may be well-approximated by the Gaussian. One example is shown in Figure 5, and rather good quality of this approximation can

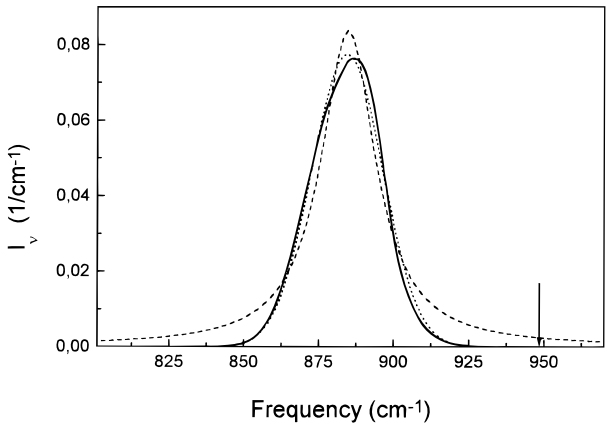

Figure 5. Fit of the calculated upward transition spectrum in the ν_3 mode of SF_6 (solid line) by the Gaussian (dotted line) and Lorentzian (dashed line); $E_{vib} = 20000$ cm^{-1}, $2\sigma_{Gw} = 3.6$ cm^{-1}.

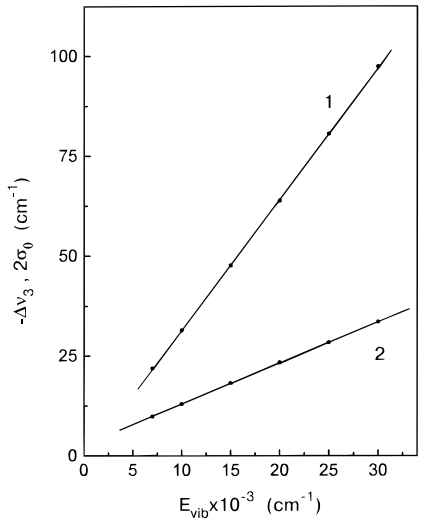

Figure 6. Shift $\Delta\nu_3$ (line 1) of the mean frequency of the upward transitions in the ν_3 mode of SF_6 and width $2\sigma_0$ (line 2) of the spectral contour as functions of the vibrational energy.

be seen there; another less satisfactory trial to approximate the calculated spectrum by the Lorentzian is shown for comparison.

Next, the dependences of the spectral-contour parameters are presented. It should be mentioned that, for each energy E_{vib} of SF_6, the histogram was calculated several times to estimate the accuracy of calculations and find its parameters such as the mean frequency $\bar{\nu}$, standard deviation σ_0, and integral intensity I_0. So, the points on the plots, giving the contour parameters, are obtained by averaging over several computation runs. Figure 6 shows the dependences of the mean frequency (in terms of its shift $\Delta\nu_3$ from the fundamental frequency ν_3) and contour width $2\sigma_0$ on the energy E_{vib}. Formally calculated in the course of the histogram generation, these parameters are in good agreement with the best-fit Gaussian ones. It is seen that both dependences exhibit very closely the linear law.

The linear dependence for the shift of the mean frequency $\bar{\nu}$ of any vibrational band from the corresponding fundamental mode frequency ν_i, i.e. $\Delta\nu_i = \bar{\nu} - \nu_i$, is frequently explored in literature in the form

$$\Delta\nu_i = \bar{X}_i \frac{E_{vib}}{\nu_i} \tag{13}$$

where $\bar{X}_i$ is an "average" anharmonicity constant. In the case under consideration this average anharmonicity constant can be

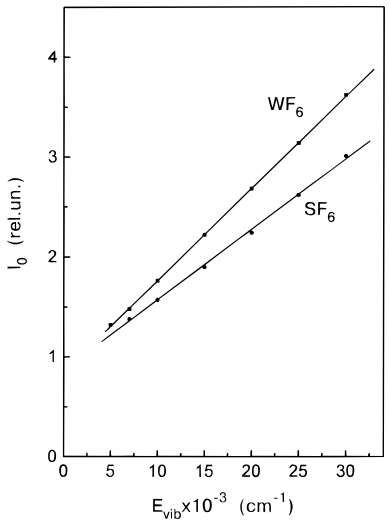

Figure 7. Integral intensity of the upward transitions in the ν_3 mode of SF_6 and WF_6 molecules as a function of the vibrational energy. This intensity I_0 is given in the relative units of that of the $0 \rightarrow 1$ transition.

obtained from the slope of the $\Delta\nu_3(E_{vib})$ dependence in Figure 6, which gives the value $\bar{X}_3 = -3.11 \pm 0.01$ cm^{-1}. For interpretation of this linear law, it is ordinarily assumed that the vibrational energy is *uniformly* distributed among all vibrational degrees of freedom. Then some simple formulas expressing the $\bar{X}_i$ through the spectroscopic constants may be derived. In our particular case of the 3-fold degenerate mode ν_3 the formula of such a kind is

$$\bar{X}_3 \approx (\sum_{i=1}^{6} g_i)^{-1} \left(8X_{33} + 4G_{33} + \sum_{i=1(i\neq 3)}^{6} g_i \frac{\nu_3}{\nu_i} X_{3i} \right) \quad (14)$$

This gives, after the substitution of the SF_6 constants, the value $\bar{X}_3 = -3.136$ cm^{-1}, which agrees well with the $\bar{X}_3$ found from Figure 6.

The standard deviation σ_0 characterizes the contour width; namely, if the contour is approximated by the Gaussian, it is equal to the halfwidth at the $e^{-1/2}I_{max}$ level. One can notice that the full width $2\sigma_0$ is rather high, changing from 9.9 cm^{-1} for $E_{vib} = 7000$ cm^{-1} to 33.6 cm^{-1} for $E_{vib} = 30\,000$ cm^{-1} near the dissociation limit. It is, at least, much wider than the assumed homogeneous width $2\gamma_L$ being used in the convolution procedure (the γ_L values are shown in the caption to Figure 4).

The normalized integral intensity of the spectrum $I_0(E_{vib})$ (see Figure 7) coincides well with the theoretical prediction $I_0(E_{vib}) = (\bar{n}_3 + 3)/3$, where $\bar{n}_3(E_{vib})$ is the average occupation number in the ν_3 mode for the energy E_{vib}.

It should be noted that all above calculations were performed with the inclusion of the anharmonic shifts in the state selection procedure (see section 3.1). We have checked the influence of this on the final results and found that the use of harmonic energies does not lead to significant errors. For example, at the highest E_{vib}, the errors are 3.8% for $\Delta\nu_3$, 7.0% for σ_0, and 1.9% for I_0. In the ν_1 mode case considered in the next subsection, the similar errors are, respectively, 4.9%, 2.6%, and 2.8%.

4.2. Mode ν_1. In the case of the mode ν_1, we deal, in fact, with the Stokes Raman transitions. The histograms of their intensity distribution (see Figure 8) look somewhat different compared to the histograms in Figure 3. Now, the groups of spectral lines with equal intensity, i.e. related to the same generated occupation number n_1, are clearly seen. Also, these

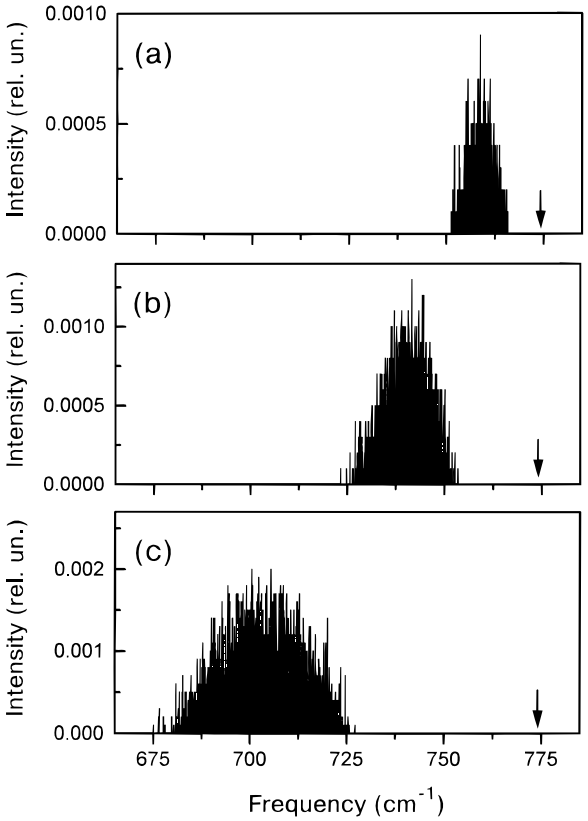

Figure 8. Histograms of the intensity distribution of the Raman Stokes transitions in the ν_1 mode of SF_6 for different vibrational energies: (a) 7000 cm^{-1}; (b) 15000 cm^{-1}; (c) 30000 cm^{-1}. The fundamental frequency is indicated by the arrow.

histograms are narrower and more asymmetric than those for the transitions in the mode ν_3. All these facts indicate what may be expected for the nondegenerate mode, whereas the anharmonic splitting in the degenerate mode ν_3 makes the spectrum broader and more symmetric. Let us clarify this.

As said, any group of the spectral lines with equal intensity joins the transitions from the states with the same n_1 and gives some fragment to the histogram. It is seen from Figure 8 that the fragment width becomes less for larger n_1. This can be easily understood as long as the energy in the other modes diminishes at the same time (the total energy E_{vib} remains constant), so deviation of the transition frequencies diminishes, too. The weight centers (mean frequencies) of different fragments do not coincide, in general. The sign of this shift of the $n_1 + 1$ fragment with respect to the n_1 fragment depends on the relations between the intramode anharmonicity constant X_{11} and the intermode anharmonicity constants X_{1i}; it is positive in the case under consideration, so one can see a sharper blue edge for the histogram. Similar behavior could be expected for the transition spectra in the mode ν_3 if there were no anharmonic splittings. With the splitting, however, each n_3 fragment becomes wider; moreover, this additional width grows with the n_3, and any histogram asymmetry disappears.

The calculated histograms were processed as previously. The distinction was that their convolution with only the narrow Gaussian window was carried out, since there are no indications in literature of the IVR rate of the mode ν_1. The resulting spectral contours are shown in Figure 9. It is seen that these contours are narrower and less red-shifted than in the case of the mode ν_3. This is because of smaller values of the X_{1i} anharmonicity constants. One can also see in Figure 10 that, as in the case of the mode ν_3, the spectral contour is

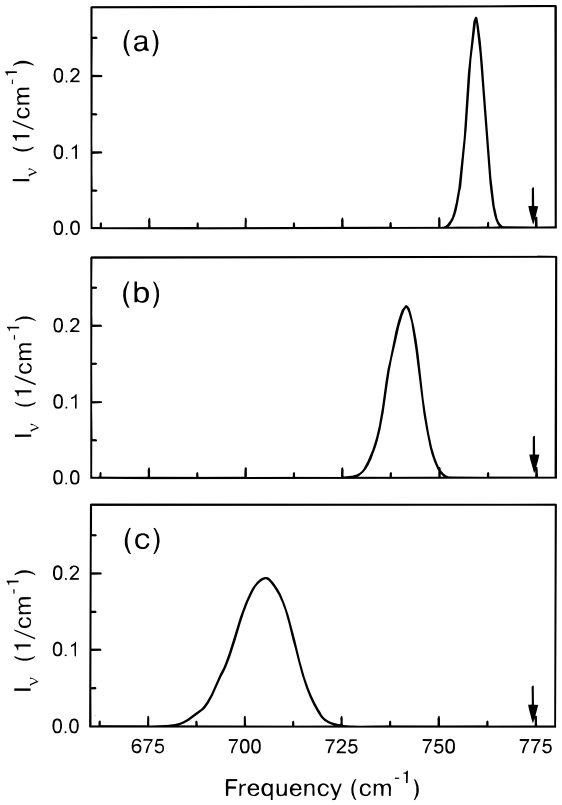

Figure 9. Raman Stokes spectra in the ν_1 mode of SF_6 for different vibrational energies: (a) 7000 cm^{-1}; (b) 15000 cm^{-1}; (c) 30000 cm^{-1}. They result from convolution of the histograms in Figure 8 with the Gaussian windows of the width $2\sigma_{Gw}$ equal to 1.2 cm^{-1} (a), 1.6 cm^{-1} (b), and 2.8 cm^{-1} (c).

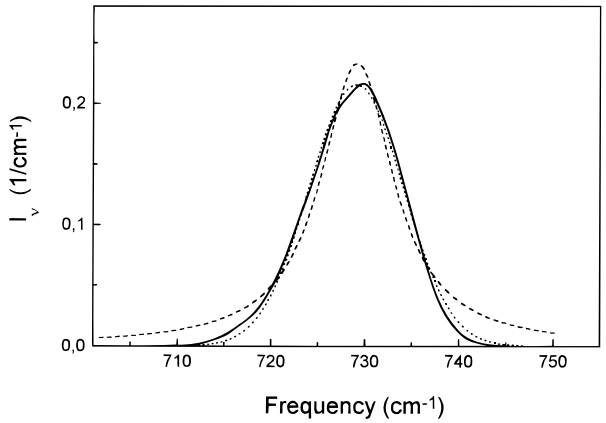

Figure 10. Fit of the calculated Raman Stokes spectrum in the ν_1 mode of SF_6 (solid line) by the Gaussian (dotted line) and Lorentzian (dashed line); $E_{vib} = 20000$ cm^{-1}, $2\sigma_{Gw} = 2$ cm^{-1}.

approximated rather well by the Gaussian. Approximation by the Lorentzian is worse.

The shift $\Delta\nu_1$ of the contour maximum and the contour width $2\sigma_0$ are shown in Figure 11 as functions of the energy E_{vib}. The average anharmonicity constant $\bar{X}_1 = -1.85 \pm 0.01$ cm^{-1} can be found from the slope of the first of these dependences (see eq 13 and related discussion). The approximate formula, like eq 14 for the 3-fold degenerated mode ν_3, is now

$$\bar{X}_1 \approx (\sum_{i=1}^{6} g_i)^{-1} \left(4X_{11} + \sum_{i=2}^{6} g_i \frac{\nu_1}{\nu_i} X_{1i} \right) \qquad (15)$$

It gives the value $\bar{X}_1 = -1.873$ cm^{-1}.

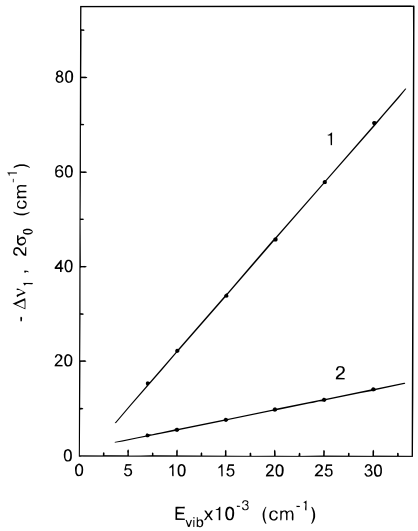

Figure 11. Shift $\Delta\nu_1$ (line 1) of the mean frequency of the Raman Stokes transitions in the ν_1 mode of SF_6 and width $2\sigma_0$ (line 2) of the spectral contour as functions of the vibrational energy.

The width $2\sigma_0$ is narrower than for the transitions in the mode ν_3 at the same vibrational energy and grows from 4.4 cm^{-1} for $E_{vib} = 7000$ cm^{-1} up to 14.2 cm^{-1} for $E_{vib} = 30\,000$ cm^{-1}. Nevertheless, these widths are again much wider than the $2\gamma_L$ for the mode ν_3. The integral normalized intensity I_0 must follow the $\bar{n}_1 + 1$ prediction as the function of the vibrational energy, and it does.

Concluding this section, we stress its principal result: the widths of the SF_6 spectra in the modes ν_3 and ν_1 are determined mainly by the effect of statistical inhomogeneous broadening.

5. Results for the Molecule WF_6

The developed model of statistical inhomogeneous broadening is applied here to another molecule of the XY_6 type, namely, WF_6. The tungsten atom is approximately 6 times heavier than the sulfur atom, and this results in considerable change of spectral parameters of the fundamental modes. The effect of central atom substitution on the spectral features is studied in this section.

5.1. Spectroscopic Parameters of WF_6. This molecule is studied much less than the SF_6. We sought complete sets of the anharmonic constants for different modes and succeeded only for the mode ν_3. Unfortunately, we did not find anywhere the experimentally measured values of intramode anharmonic constants G_{33} and T_{33}, which are responsible for splittings of the ν_3 mode energy levels. Only computed values are available from ref 44, which are probably somewhat smaller than the actual existing ones. The latter may be deduced by comparing the SF_6 constants computed in the same ref 44 with the experimental values. Nevertheless, we have preferred to use, for definiteness, the complete set of anharmonic constants $\{X_{33}, G_{33}, T_{33}\}$ from the same ref 44 rather than extract one of them, X_{33}, from any other source (for example, X_{33} was measured in ref 45). As for the other spectroscopic constants, the X_{3i} and the ν_i have been taken from ref 45, except the more precise ν_3, which was taken from ref 46. The spectroscopic constants that are explored in the present calculations are listed in Table 2.

5.2. Mode ν_3. The onset of the vibrational chaos in the molecule WF_6 is unknown, but supposedly lies lower than in SF_6 because of smaller normal mode frequencies. So, our simulations started from the energy $E_{vib} = 5000$ cm^{-1}. As long

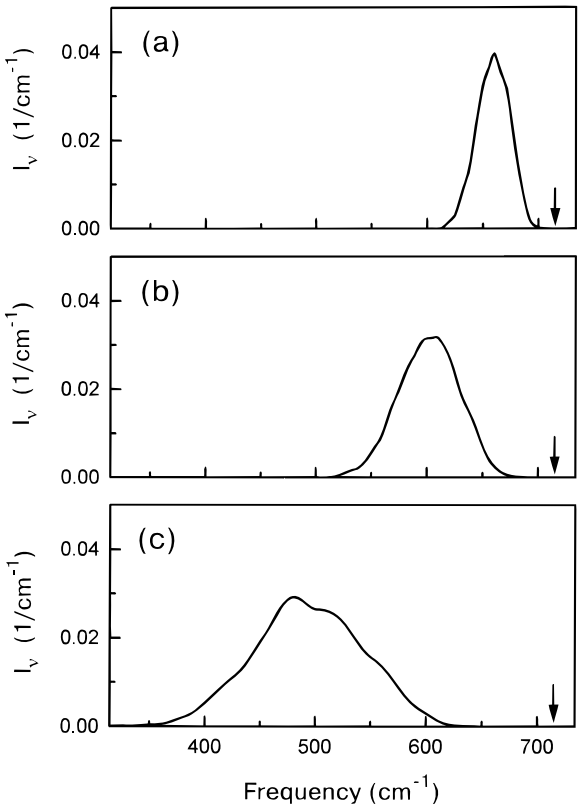

Figure 12. Upward transition spectra in the ν_3 mode of WF_6 for different vibrational energies: (a) 7000 cm^{-1}; (b) 15000 cm^{-1}; (c) 30000 cm^{-1}. They result from convolution of the corresponding histograms with the Gaussian windows of the width $2\sigma_{Gw}$ equal to 4.5 cm^{-1} (a), 8 cm^{-1} (b), and 15 cm^{-1} (c).

TABLE 2: WF_6 Spectroscopic Constants (in cm^{-1}) Used for Calculations

i	ν_i	X_{3i}
1	772.1	−1.7
2	678.2	−3.5
3	713.9152	$X_{33} = -0.63$ $G_{33} = 0.21$ $T_{33} = -0.105$
4	252.1	−0.5
5	320	−4.4
6	129	−2

as the anharmonicity constants of WF_6 are not known in full, we have calculated only harmonic energies of vibrational states for their selection. Figure 12 shows the inhomogeneous spectra after processing the histograms. These spectra are for the same energies as the previously shown spectra for also the mode ν_3, but of SF_6 (see Figure 4). Now the spectra are about 3 times broader and more red-shifted; this may be understood from the fact that the excitations of the low-frequency modes of WF_6, due to large anharmonicity constants, lead to larger frequency shifts than in SF_6. The spectral contour parameters $\Delta\nu_3$ and $2\sigma_0$ depending on the energy E_{vib} are shown in Figure 13. The average anharmonicity constant for the mode ν_3 of WF_6 can be found from the $\Delta\nu_3(E_{vib})$ slope: $\bar{X}_3 = -5.04 \pm 0.01$ cm^{-1}. The approximate formula eq 20 gives a rather close value: $\bar{X}_3 = -5.34$ cm^{-1}.

The integral normalized intensity is shown in Figure 7. As for SF_6, it follows the formula $(\bar{n}_3 + 3)/3$ rather accurately.

There are no indications of the IVR rates in WF_6 anywhere in the literature. Nevertheless, numerically large inhomogeneous widths given by our simulations enable one to assume that the inhomogeneous contribution should be dominant.

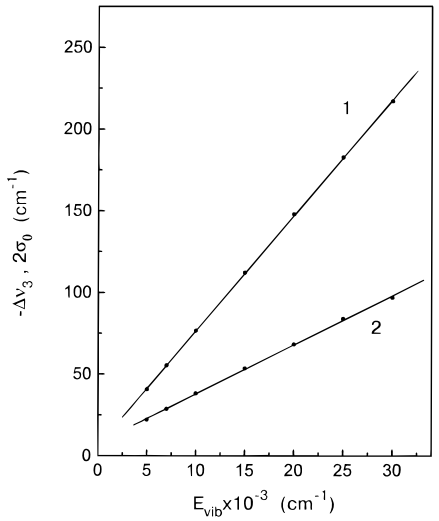

Figure 13. Shift $\Delta\nu_3$ (line 1) of the mean frequency of the upward transitions in the ν_3 mode of WF_6 and width $2\sigma_0$ (line 2) of the spectral contour as functions of the vibrational energy.

Our final note concerns individual roles of scalar (mainly intermode) anharmonicity and anharmonic splitting in the formation of the inhomogeneous contour width. Looking at the values of the anharmonicity constants, one may assume that the anharmonic splitting is not very important in the specific case of WF_6. The direct calculation confirms this assumption. Another situation takes place for the same mode ν_3, but of SF_6. There, these two effects give approximately equal contributions to the width. We shall discuss this point further in section 7.

6. Effect of Rotations on the Band Shapes

The above considered spectra involve only vibrational transitions but do not include any rotational substructure nor its dependence on the rotational quantum number J. Two effects can be added to the previous treatment in the same approximation order. They are the rotor energy, which results in different frequencies of the transitions in different rotational branches, and Coriolis splitting in the 3-fold degenerate modes, which strongly modifies the transition spectra therein. One next order effect, which is the change of the rotational constant B for the excited vibrational states in accordance with

$$B_{n_i} = B_0 + \alpha_i n_i \tag{16}$$

can be easily taken into account, too.

Only the latter of the mentioned effects influences spectra of the Raman transitions in the totally symmetric mode ν_1. Indeed, only the Q-branch ($\Delta J = 0$) is allowed for these transitions, and no Coriolis effect is present in the states of this nondegenerate mode. Thus, the frequency of transition from any selected state in our calculation procedure is just shifted from the previously used one by the value $\alpha_1 J(J + 1)$, and this shift does not depend on the generated mode occupation numbers. Numerically, for SF_6, the value of this shift is about 1 cm^{-1} for the typical room-temperature $J \approx 50$ cm^{-1}, i.e. small with respect to the $\Delta\nu_1$ shifts shown in Figure 11.

More complex changes may be expected, in general, for the infrared transitions in the mode ν_3. The previously calculated spectra formally correspond to the situation when both rotational constant B and Coriolis constant ζ_3 are equal to zero.

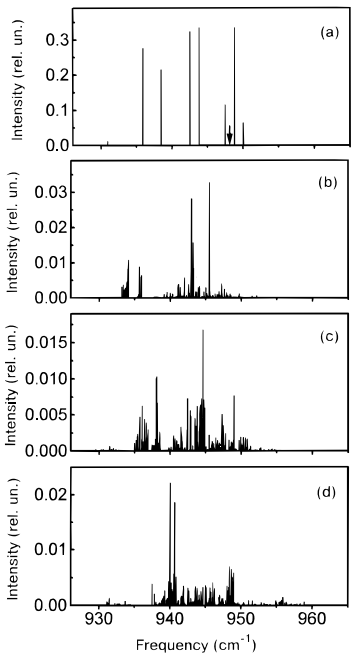

Figure 14. Spectra of the $n_3 = 2 \rightarrow n_3 = 3$ transitions in the ν_3 mode of SF_6. (a) Purely vibrational spectrum; the arrow indicates the frequency of the $n_3 = 0 \rightarrow n_3 = 1$. (b−d) Vibration−rotation spectra for the states with $J = 15$ at $n_3 = 2$ in different rotational branches: (b) in the P-branch, (c) in the Q-branch, (d) in the R-branch.

The nonzero B and ζ_3 results in the trivial fact of redistribution of the full intensity I_0 of the calculated spectra into three rotational P-, Q-, and R-branches having different mean frequencies. Their intensities are

$$I_P = \frac{2J-1}{3(2J+1)} I_0, \quad I_Q = \frac{1}{3} I_0, \quad I_R = \frac{2J+3}{3(2J+1)} I_0 \quad (17)$$

For the shifts of their mean frequencies from the previously calculated values caused by the rotation and Coriolis interaction, there appears the common shift for all three branches $\Delta\nu_{Cor} \approx -B\zeta_3(\bar{n}_3 + 2)$ and shifts for the P- and R-branches

$$\Delta\nu_P \approx -2(1-\zeta_3)BJ$$

$$\Delta\nu_R \approx 2(1-\zeta_3)B(J+1) \quad (18)$$

which are responsible for the usual PQR-structure of the vibrational band. The main complication, however, may arise from the fact that the spectrum of any $(n_3, J) \rightarrow (n_3 + 1, J')$ manifold of transitions is in reality (i.e., with $\zeta_3 \neq 0$) much more complex than the spectrum of purely vibrational transitions (with $\zeta_3 = 0$).

One illustration is shown in Figure 14. Four spectra of $n_3 = 2 \rightarrow n_3 = 3$ transitions are presented in this figure. The spectrum in Figure 14a is one of the fragmentary spectra involved in our calculations of section 4.1 for the molecule SF_6 when any state with $n_3 = 2$ is generated, as discussed in section 3. Three other spectra in this figure are for the $(n_3 = 2, J = 15) \rightarrow (n_3 = 3, J = 14)$ transitions (b), $(n_3 = 2, J = 15) \rightarrow (n_3 = 3, J = 15)$ transitions (c), and $(n_3 = 2, J = 15) \rightarrow (n_3 = 3, J = 16)$ transitions (d). These spectra are obtained by the diagonalization of the vibration−rotation Hamiltonian $\hat{H}_{\nu_3}$ of the mode ν_3, which includes the ν_3-related terms of the Hamiltonian eq 9, the purely rotational terms, and the Coriolis interaction terms. This Hamiltonian is

$$\hat{H}_{\nu_3} = X_{33}\hat{n}_3(\hat{n}_3 - 1) + G_{33}(\hat{\mathbf{l}}_3^{\,2} - \hat{n}_3) + T_{33}\hat{O}_{33}(\text{tensor}) + (B + \alpha_3\hat{n}_3)\hat{\mathbf{J}}^2 + B\zeta(\hat{\mathbf{J}}\cdot\hat{\mathbf{l}}_3) \quad (19)$$

with the anharmonicity constants X_{33}, G_{33}, and T_{33} of section 4 and the vibrational and Coriolis constants from ref 37: $B = 0.091\,084\ \text{cm}^{-1}$, $\alpha_3 = -1.3106 \times 10^{-4}\ \text{cm}^{-1}$, and $\zeta_3 = 0.69344$. As the $\hat{H}_{\nu_3}$ diagonalization result, one has the splittings of the (n_3, J) manifolds onto the nondegenerate levels of symmetry A_1 or A_2, 2-fold degenerate levels of symmetry E, and 3-fold degenerate levels of symmetry F_1 or F_2. Then, having the eigenvectors in the symmetry-adapted basis (see basically ref 47 and also ref 48 for some details) and exploiting the Moret−Bailly selection rules,[47] one can calculate the intensities of allowed dipole transitions, which are, in principle, all the transitions between the states of the same symmetry; in addition, the frequencies of allowed transitions are found from the eigenvalues. After that, all the initial states (with $n_3 = 2$ and $J = 15$ in our case of Figure 14) are assumed to be populated proportionally to their degeneracies, and the resulting spectra, as shown in Figure 14, are produced.

Now, two questions arise: to what extent do really more complicated fragmentary spectra modify the previous results of section 4.1, and how different are the spectra for the initial states with different J? To answer these questions, we performed the calculations of the inhomogeneous spectra in the mode ν_3 with $J = 15$ and $J = 40$ in a wide range of vibrational energy. For these calculations, the state selection procedure was the same as used previously, but new, much more complex $(n_3, J) \rightarrow (n_3 + 1, J')$ transition spectra were used. The resulting spectra appear to be again nearly Gaussian, with the widths even a little narrower (e.g., about 3% for the energy 10 000 cm^{-1}) than those plotted in Figure 6. The intensity is distributed among the rotational branches in perfect correspondence with eq 17. The mean frequencies of the different rotational branches perfectly agree with eq 18. So, the principal conclusion from these simulations is that the vibration−rotation spectra can be produced by the purely vibrational spectra: some differences for different J in the width can be neglected, and some differences for different J in the integral intensity and mean frequency can be taken into account systematically using eqs 17 and 18.

Our final point refers to the physical reasons for the small effect of the Coriolis splitting on the spectral width. For the spectra shown in Figure 14, for example, the standard deviation that characterizes the width is 4.71 cm^{-1} for the spectrum in Figure 14a and 4.56 cm^{-1} for the spectra in Figure 14b−d. It can be derived that the standard deviation σ_{n_3} of the $n_3 \rightarrow n_3 + 1$ transition spectrum in any rotational branch may be schematically presented as

$$\sigma_{n_3} = (\overline{\nu_T^{\,2}} + \overline{\nu_l^{\,2}} - \bar{\nu}^2)^{1/2} \quad (20)$$

That is, the mean value of the squared frequency is the sum of two terms: the first term $\overline{\nu_T^{\,2}}$ is determined by the matrix elements of the operator $\hat{O}_{33}$ (tensor) and is therefore proportional to $T_{33}^{\,2}$, whereas the second term $\overline{\nu_l^{\,2}}$ is determined by the l-splitting of the symmetry-adapted basis states and is proportional to the value of $(G_{33} - B\zeta_3)^2$. Hence one can easily see that the effect of the Coriolis interaction on the width is small if the ratio $B\zeta_3/G_{33}$ is small. (In the SF_6 case, this ratio is 0.068.)

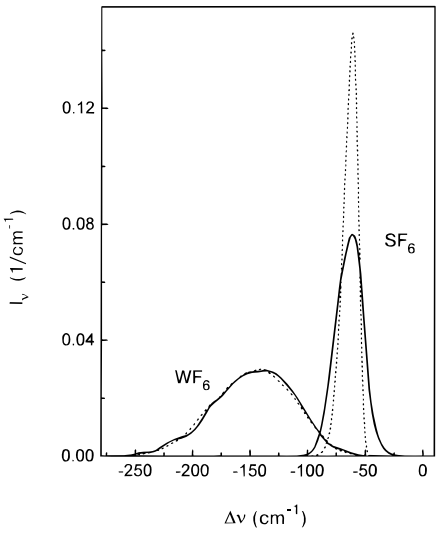

Figure 15. Spectra of the upward transitions in the ν_3 mode of two molecules with the inclusion of the anharmonic splitting (solid line) and without it (dotted line); $E_{vib} = 20000$ cm^{-1}. Zero frequency shift in the $\Delta\nu_3$ axis refers to the fundamental frequencies 948.1025 cm^{-1} for SF_6 and 713.9152 cm^{-1} for WF_6.

Moreover, as long as the signs of G_{33} and ζ_3 are opposite, the Coriolis effect reduces the width as confirmed by the direct calculation.

7. Discussion and Conclusions

The results of our simulations for the molecules SF_6 and WF_6 led us to consider the inhomogeneous broadening as, at least, the important effect in formation of the spectra of vibration−rotation transitions between highly excited states. The presented computational scheme has proved to be rather simple and reliable in view of several independent tests. It provides the integral intensities and peak positions very accurately in a wide range of vibrational energy from the onset of chaos up to the dissociation limit. The obtained bandwidths are much wider than those presumably caused by IVR. For the latter aspect, it should be noted that we can directly compare the widths calculated in this work with only the much narrower IVR widths for the mode ν_3 of SF_6 suggested in ref 34, but large calculated widths for the mode ν_1 of SF_6 and the mode ν_3 of WF_6, too, make the assumption for their dominant role very realistic.

The Raman ν_1 band in the XY_6 type molecules is inhomogeneously broadened because of different anharmonic shifts for the excited vibrational states with different mode occupation numbers. For the infrared band ν_3, the additional effect of splitting of the states of the 3-fold degenerate mode ν_3, due to its internal anharmonicity (see section 3.2), may be significant. Its relative role can be found in the course of calculation. Figure 15 gives one illustration for the energy 20 000 cm^{-1} which shows that the contribution to the width from the anharmonic splitting is about 45% in the case of SF_6 and only about 1% in the case of WF_6. This difference is not more than the anharmonicity-constant interplay (see also the discussion at the end of section 5).

For future applications, it is useful to compare the widths calculated in this work for the mode ν_3 of SF_6 with those estimated analytically in ref 34. The values for the width are presented there for both situations, *without* and *with* the anharmonic splitting, so it is natural to compare them with our corresponding values (as found, for example, from the dotted and solid spectral contours in Figure 15). Such comparison shows that our "unsplit" values are 2.7 times more at $E_{vib} = 7000$ cm^{-1} and 2.0 times more at $E_{vib} = 30\,000$ cm^{-1} than the corresponding values of ref 34. It may be supposed that the noticed difference is due to the equipartitioning of the vibrational energy among the modes, assumed in ref 34. Since this assumption is more valid for high energies, better coincidence may be expected as the energy grows. This is really so, but the discrepancy is still large even at the dissociation limit. Moreover, being applied to the mode ν_3 of WF_6, the analytical evaluation works much worse: it gives 5 times less values for $E_{vib} = 30\,000$ cm^{-1} and 7 times less values for $E_{vib} = 5000$ cm^{-1} than the calculated ones.

The contribution to the width from the ν_3 anharmonic splitting estimated in ref 34 almost compensates the discrepancy with the calculation results of this work, but we believe that this fact is situational; really, the difference between the analytical evaluation and direct calculation for the ν_3 mode of WF_6 is very large: 4.5 times at $E_{vib} = 5000$ cm^{-1} and 3 times at $E_{vib} = 30\,000$ cm^{-1}.

We stress the comparison of the results of this work with the previous analytical estimates because the same effects are involved in both approaches. In reality, however, some other effects may add to the values of the widths. For example, it may occur that occasional anharmonic intermode resonances lead to redistribution of the intensity from the $n_a \rightarrow n_a + 1$ transition to some close combination transitions. In the case of SF_6, disturbance of both the ν_1 and ν_3 bands may be caused by the close intermode resonance $\nu_1 + \nu_5 \approx \nu_3 + \nu_6$ (with a defect of about 3 cm^{-1}) depending on the related anharmonicity constant value. Another effect may originate from nonzero intermode anharmonicity constants G_{ij}, T_{ij}, and S_{ij} and lead to additional broadening of spectra of transitions in degenerate modes, as mentioned at the end of section 3.2. It should be noted that it was not computationally easy to implement the mentioned effects for the molecules like XY_6, even if all the constants are known, because of the enormous degeneracy of high vibrational states leading to the necessity of diagonalization of very large matrices for any selected state. The approaches to do this rather accurately in some indirect way are in progress now.

As for the experimental verification of the presented calculation results, we can refer to our coming publication.[49] The Raman spectrum of the mode ν_1 of SF_6 has been measured in the wide range of vibrational temperature from 850 K up to 1600 K, and rather good agreement has been found between the experimental results and spectra calculated with the use of the model presented here.

Concluding, we should note that any simple treatment of the transition spectra for highly vibrationally excited molecules is very desirable for modeling the infrared MPE dynamics. If the main features of such spectra are known on the basis of known spectroscopic constants, then the more realistic choice of other unknown parameters of the complicated MPE process can be made. Otherwise, the parameters of such spectra would be included in the list of unknown ones, making the MPE modeling much less convincing. We believe that the approach of this work, based on reasonable assumptions and computationally not hard, provides more correct and reliable spectroscopic data for transitions between highly vibrationally excited states than the prior ones.

Acknowledgment. This work was partially supported by the Russian Foundation for Fundamental Research. I.Yu.P. and E.A.R. thank Dr. A. L. Malinovsky for useful advice.

References and Notes

(1) (a) Isenor, N. R.; Richardson, M. C. *Appl. Phys. Lett.* **1971**, *18*, 224. (b) Isenor, N. R.; Merchant, V.; Hallsworth, R. S.; Richardson, M. C. *Can. J. Phys.* **1973**, *51*, 1281.

(2) (a) Letokhov, V. S.; Ryabov, E. A.; Tumanov, O. A. *Opt. Commun.* **1972**, *5*, 168. (b) Ambartzumian, R. V.; Chekalin, N. V.; Doljikov, V. S.; Letokhov, V. S.; Ryabov, E. A. *Chem. Phys. Lett.* **1974**, *25*, 515.

(3) (a) Ambartzumian, R. V.; Letokhov, V. S.; Ryabov, E. A.; Chekalin, N. V. *Sov. Phys.−JETP Lett.* **1974**, *20*, 273. (b) Ambartzumian, R. V.; Gorokhov, Yu. A.; Letokhov, V. S.; Makarov, G. N. *Sov. Phys.−JETP Lett.* **1975**, *21*, 171.

(4) Ambartzumian, R. V.; Letokhov, V. S. In *Chemical and Biochemical Applications of Lasers*; Moore, C. B., Ed.; Academic Press: New York, 1977; Vol. 3, p 166.

(5) Bloembergen, N.; Yablonovich, E. *Phys. Today* **1978**, *31* (5), 23.

(6) Schulz, P. A.; Sudbo, Aa. S.; Krajnovich, D. J.; Kwok, H. S.; Shen, Y. R.; Lee, Y. T. *Annu. Rev. Phys. Chem.* **1979**, *30*, 379.

(7) Letokhov, V. S.; Makarov, A. A. *Sov. Phys.−Uspekhi* **1981**, *24*, 366.

(8) King, D. S. In *Dynamics of the Excited State*; Lawley, K. P., Ed.; Wiley: New York, 1982; p 105.

(9) Bagratashvili, V. N.; Letokhov, V. S.; Makarov, A. A.; Ryabov, E. A. *Multiple Photon Infrared Photophysics and Photochemistry*; Harwood Acad. Publ.: Chur, Switzerland, 1985.

(10) *Multiple-Photon Excitation and Dissociation of Polyatomic Molecules*; Cantrell, C. D., Ed.; Springer: Berlin, 1986.

(11) Lyman, J. L. In *Laser Spectroscopy and its Applications*; Radziemski, L. J., Solarz, R. W., Raisner, J. A., Eds.; Dekker: New York, 1987; p 417.

(12) Lupo D. W.; Quack, M. *Chem. Rev.* **1987**, *87*, 181.

(13) *Innovative Laser Technologies in Nuclear Energy. Proceedings of the 6th International Symposium on Advanced Nuclear Energy Research*; March 23−25, 1994, Mito, Ibarakie, Japan; JAERI: Japan, 1994.

(14) Bagratashvili, V. N.; Doljikov, V. S.; Letokhov, V. S.; Makarov, A. A.; Ryabov, E. A.; Tyakht, V. V. *Sov. Phys.−JETP* **1979**, *50*, 1075.

(15) Dübal, H.-R.; Quack, M. *J. Chem. Phys.* **1984**, *81*, 3779.

(16) Stuchebrukhov, A.; Ionov, S.; Letokhov, V. *J. Phys. Chem.* **1989**, *93*, 5357.

(17) Stuchebrukhov, A. A.; Marcus, R. A. *J. Chem. Phys.* **1993**, *98*, 6044.

(18) Lubich, L.; Boyarkin, O. V.; Settle, R. D. F.; Perry, D. S.; Rizzo, T. R. *Faraday Discuss.* **1995**, *102*, 167.

(19) Demianenko, A.; Letokhov, V.; Makarov, A.; Ryabov, E. *Faraday Discuss.* **1995**, *102*, 301.

(20) Evseev, A. V.; Krivtsun, V. M.; Kuritsyn, Yu. A.; Makarov, A. A.; Puretzky, A. A.; Ryabov, E. A.; Snegirev, E. P.; Tyakht, V. V. *Chem. Phys.* **1986**, *106*, 131.

(21) (a) Bagratashvili, V. N.; Ionov, S. I.; Letokhov, V. S.; Lokhman, V. N.; Makarov, G. N.; Stuchebrukhov, A. A. *Sov. Phys.−JETP* **1987**, *66*, 670; (b) *Chem. Phys. Lett.* **1988**, *146*, 599.

(22) Boyarkin, O. V.; Ionov, S. I.; Bagratashvili, V. N. *Chem. Phys. Lett.* **1988**, *146*, 106.

(23) Fleming, P. R.; Li, M.; Rizzo, T. R. *J. Chem. Phys.* **1991**, *94*, 2425.

(24) *Laser Spectroscopy of Highly Vibrationally Excited Molecules*; Letokhov, V. S., Ed.; Adam Hilger: Bristol, 1989.

(25) Nesbitt, D. J.; Field, R. W. *J. Phys. Chem.* **1996**, *100*, 12735.

(26) Boyarkin, O. V.; Ionov, S. I.; Kobakhidze, A. A. *Spectrochim. Acta* **1990**, *46A*, 537.

(27) (a) Kuzmin, M. V.; Letokhov, V. S.; Stuchebrukhov, A. A. *Sov. Phys.−JETP* **1986**, *63*, 264. (b) Kuzmin, M. V.; Stuchebrukhov, A. A. In ref 24; p 178.

(28) Kubo, R. In *Fluctuation, Relaxation and Resonance in Magnetic Systems*; Haar, D. Ter, Ed.; Oliver and Boyd: Edinburgh, 1962; p 23.

(29) Dicke, R. *Phys. Rev.* **1953**, *89*, 472.

(30) Nitzan, A.; Persson, B. N. J. *Chem. Phys.* **1985**, *83*, 5610.

(31) (a) Makarov, A. A.; Tyakht, V. V. *Sov. Phys.−JETP* **1987**, *63*, 9. (b) Makarov, A. A. In ref 24; p 106.

(32) Bagratashvili, V. N.; Burimov, V. N.; Ionov, S. I.; Sviridov, A. P.; Stuchebrukhov, A. A.; Turovetz, I. M. *Chem. Phys. Lett.* **1987**, *137*, 45.

(33) (a) Dübal, H.-R.; Quack, M. *Chem. Phys. Lett.* **1980**, *72*, 342. (b) Baggot, J. E.; Chuang, M.-C.; Zare, N.; Dübal, H.-R.; Quack, M. *J. Chem. Phys.* **1985**, *82*, 1186.

(34) Angelié, C. *J. Chem. Phys.* **1993**, *98*, 2541.

(35) Rice, S. A. In *Photoselective Chemistry, Part 1*; Jortner, J., Levine, R. D., Rice, S. A., Eds.; Advances in Chemical Physics, Vol. 47; Wiley: New York, 1981; p 117.

(36) Hecht, K. T. *J. Mol. Spectrosc.* **1960**, *5*, 355.

(37) Bobin, B.; Bordé, C. J.; Bordé, J.; Bréant, C. *J. Mol. Spectrosc.* **1987**, *121*, 91.

(38) McDowell, R. S.; Krohn, B. J.; Flicker, H.; Vasquez, M. C. *Spectrochim. Acta* **1986**, *42A*, 351.

(39) Alimpiev, S. S.; Sartakov, B. G. *Laser Chem.* **1992**, *12*, 147.

(40) McDowell, R. S.; Krohn, B. J. *Spectrochim. Acta* **1986**, *42A*, 371.

(41) (a) Malinovsky, A. L.; Letokhov, V. S.; Ryabov, E. A. *Chem. Phys.* **1989**, *139*, 229. (b) Ryabov, E. A. In ref 24; p 55.

(42) Becker, F. S.; Kompa, K. L. *Nucl. Technol.* **1982**, *58*, 329.

(43) Angelié, C. *J. Chem. Phys.* **1992**, *96*, 8072.

(44) Halonen, L.; Child, M. S. *J. Chem. Phys.* **1983**, *79*, 559.

(45) McDowell, R. S.; Asprey, L. B. *J. Mol. Spectrosc.* **1973**, *48*, 254.

(46) Takami, M.; Kuze, H. *J. Chem. Phys.* **1984**, *80*, 5994.

(47) Moret-Bailly, J. *J. Mol. Spectrosc.* **1965**, *15*, 344.

(48) Cantrell, C. D.; Letokhov, V. S.; Makarov, A. A. In *Coherent Nonlinear Optics. Recent Advances*; Feld, M. S., Letokhov, V. S., Eds.; Topics in Current Physics, Vol. 21; Springer: Berlin, 1980; p 165.

(49) Malinovsky, A. L.; Petrova, I. Yu., Ryabov, E. A.; Makarov, A. A.; Letokhov, V. S. To be published.